DOE/ER/13394-T3

STUDIES OF AUTOIONIZING STATES RELEVANT TO DIELECTRONIC RECOMBINATION

Progress Report

July 1, 1991 - June 30, 1994

T.F. Gallagher

Department of Physics
University of Virginia
Charlottesville, VA 22901

December, 1993

PREPARED FOR THE U.S. DEPARTMENT OF ENERGY
UNDER GRANT NUMBER: DEFG05-85ER13394

DISCLAIMER

Portions of this document may be illegible in electronic image products. Images are produced from the best available original document.

Table of Contents

Reprints / Preprints — removed

I. Introduction

The goal of this research program supported by grant DEFG05-85-ER13394 is to study the properties of autoionizing states to understand in detail dielectronic recombination of ions and electrons. Recombination of ions and electrons in a plasmas determines many of the properties of the plasma.[1,2] For slow electrons recombination occurs through radiative recombination, but the recombination of fast electrons is often via dielectronic recombination. As an example, dielectronic recombination of a ground state Mg^+ ion and an electron can occur by the process

$$e^- + Mg^+ \rightarrow Mg\ 3pn\ell \rightarrow Mg\ 3sn\ell + h\nu. \qquad (1)$$

The process occurs as follows. An electron with an energy just below the Mg^+ 3s-3p interval impinges on the Mg^+ 3s ion and excites it to the 3p state. In so doing it loses the Mg^+ 3s-3p energy to the Mg^+ and, as result, becomes slightly bound in its coulomb potential, creating the doubly excited Mg $3pn\ell$ state. If an atom in this state decays to the $3sn\ell$ state by emitting a photon the recombination is complete, as shown in Eq. (1). If, however, it autoionizes, there is no recombination. Dielectronic recombination is important in both magnetically confined fusion and astrophysical plasmas, and it may play a role in processing plasmas. In addition, autoionizing states are of more general interest. For example, they play key roles in proposed approaches to short wavelength lasers.[3]

During the period of the present grant, July 1, 1991 - June 30, 1994, we have put substantial effort into the study of autoionizing states in Mg. The motivations are several. First, some of the cleanest measurements of dielectronic recombination have been made in Mg by Dunn and his collaborators.[4] Second, there have been recent K matrix calculations for Mg autoionizing states by Greene and his collaborators.[5,6] Finally, Mg exhibits qualitatively different spectra in the autoionizing region than do the heavier alkaline earth atoms, and a firm understanding of these spectra poses an intrinsically interesting challenge. In this report we describe the research projects carried out under the current grant.

The first topic we have investigated is the angular distribution of electrons ejected from the

autoionizing Mg 3pns and 3pnd states. Both of these sets of measurements provide more stringent tests of the K matrix calculations than do measurements of total cross sections. The second topic is the effect of static and microwave electric fields on autoionizing states. Our previous measurements in Ba have shown the profound influence of electric fields on autoionization rates and we have made extensive new measurements in both Ba and Mg. Electric fields are of real importance for dielectronic recombination, since they are present as macroscopic fields in beam experiments and as microfields in plasmas. Finally, we have begun time resolved measurements. We have set up a picosecond laser system, and we have just finished the first experiment with it. Specifically we have used picosecond excitation from a bound Mg 3pnd Rydberg wave packet to the autoionizing 3pnd states to show explicitly the correlation between the spatial location of the Rydberg electron and the frequency of the exciting light.

II. Experimental Approach

The general approach used in these experiments is multistep laser excitation of Mg atoms in a low density atomic beam, a method often called the isolated core excitation technique.[7] One of the important aspects of this approach is that we separately excite each of the two valence electrons.[7] To illustrate this approach, let us consider how we produce the autoionizing 3pns states of Mg. Initially, the Mg atoms are in the $3s^2$ ground state. Using two synchronous, pulsed dye lasers, we excite the atoms from the $3s^2$ to the 3s3p state and then from the 3s3p state to the 3sns state. Only one electron has been excited, to a very large orbit, and we call it the "outer" electron. With a third laser pulse, which must occur within the 3sns lifetime of several microseconds, we induce the 3sns → 3pns transition to the autoionizing 3pns state. In essence, we excite the inner electron from the 3s to the 3p state, while the outer electron remains a spectator in its ns orbit. The 3sns → 3pns transition is a strong transition because it is the resonance line of the Mg^+ ion, which has an oscillator strength of ~ 1,[8] with a spectator electron.

The third laser can also directly photoionize the Ba 3sns state to the 3sεp continuum. However, the photoionization cross section for a visible photon impinging upon a Rydberg state is vanishingly small.[7] Consequently, there is no observable interference between direct photoionization and excitation of the autoionizing state, which produces the asymmetric Beutler-Fano profiles usually associated with autoionizing states.[9] The excitation spectrum of the 3pns state from the 3sns state, obtained by scanning the third laser's wavelength, has a particularly simple form. It is a Lorentzian line whose center gives immediately the energy of the 3pns state and whose width gives its autoionization rate. Although we have used the excitation of the Mg 3pns states as an example, it is clear that the physics of the third transition is the same regardless of the n, ℓ state of the outer electron.

The apparatus consists of an atomic beam apparatus and a pulsed laser system. In the beam apparatus a thermal Mg beam effuses from a resistively heated oven and passes into an interaction region where it is excited by the dye laser beams. In the electron spectroscopy experiments two configurations

of detectors have been used, a pair of electron detectors 90° apart or an electron and an ion detector 180° apart. In both cases the interaction region and the detectors are enclosed in a magnetic shield to reduce the magnetic fields to less than 5 mG. In the electric field experiments a slightly different arrangement is used. For the static field experiments the interaction region is between two capacitor plates to which high voltages are applied to produce fields of up to 5 kV/cm. For the microwave field experiments the capacitor plates are replaced by a microwave cavity, and the atoms are excited inside the cavity in microwave fields of up to 1 kV/cm.

In most of the work described in this report we have used 5ns dye lasers pumped by the second harmonic of a Q switched Nd:YAG laser. The dye lasers are configured as oscillator - amplifiers, and they produce 1 mJ pulses with 1 cm^{-1} linewidths. The visible dye laser pulses are frequency doubled to the ultraviolet using angle tuned KDP crystals, yielding 100 μJ pulses. In experiments requiring higher resolution we have used a pressure tuned dye laser with a 0.1 cm^{-1} linewidth. As mentioned above, we have done one experiment with a picosecond laser, and the approach employed will be described in the next section.

III. Progress under the present grant

Angular distributions of electrons from the Mg 3pns J=1 states

These experiments were motivated by a desire to test stringently the K matrix calculations which had reproduced so well the total photoabsorption cross sections from the Mg 3sns states to the 3pns and 3pnd states.[10,11] We excited the Mg atoms from the ground $3s^2\ ^1S_0$ state to the spherically symmetric, bound Rydberg 3sns $^1S_0$ states with two dye lasers. We then excited the atoms to the $3p_j ns_{1/2}$ J=1 autoionizing states with a third, linearly polarized dye laser. Since the intermediate 3sns state is spherically symmetric the angular distribution can be expressed as[12]

$$I(\theta) = \frac{I_0}{4\pi}\left[1 + \beta P_2(\cos\theta)\right], \qquad (2)$$

where θ is the angle between the E field of the laser beam and the direction in which the electron is ejected. The β parameter, which lies between -1 and 2, describes the angular distribution. For example, β = -1 corresponds to a $\sin^2\theta$ distribution, and β=2 corresponds to a $\cos^2\theta$ distribution.

In this experiment we placed electron detectors at two values of θ 90° apart. Systematic tests were made with many values of the two angles, and the final data were collected with the detectors at Θ=0° and 90°. The final data were taken by scanning the wavelength of the third laser and recording the electron signals I(θ) for θ = 0° and 90°. Typical results are shown in Fig. 1. Two features of Fig. 1 are immediately apparent. First, as a rule more electrons come out at θ = 0° than at θ = 90°, as shown by the factor of twenty scale difference. Second, the θ = 0° and θ = 90° spectra are not the same, indicating a variation in the angular distribution with energy.

The spectral scans of Fig. 1 are easily reduced to the β parameter, as shown in Fig. 2. There are several features of Fig. 2 to note. Typically β = 2, indicating that the electrons are ejected in the direction of the laser field. There are two departures from β = 2, a broad dip at a transition energy of ~ 35680 cm^{-1}, between the Mg^+ $3s_{1/2}$ - $3p_{1/2}$ and $3s_{1/2}$ - $3p_{3/2}$ transition energies of 35669 cm^{-1} and 35761 cm^{-1}, and many sharp decreases, at the locations of other J=1 resonances. Finally, it is apparent

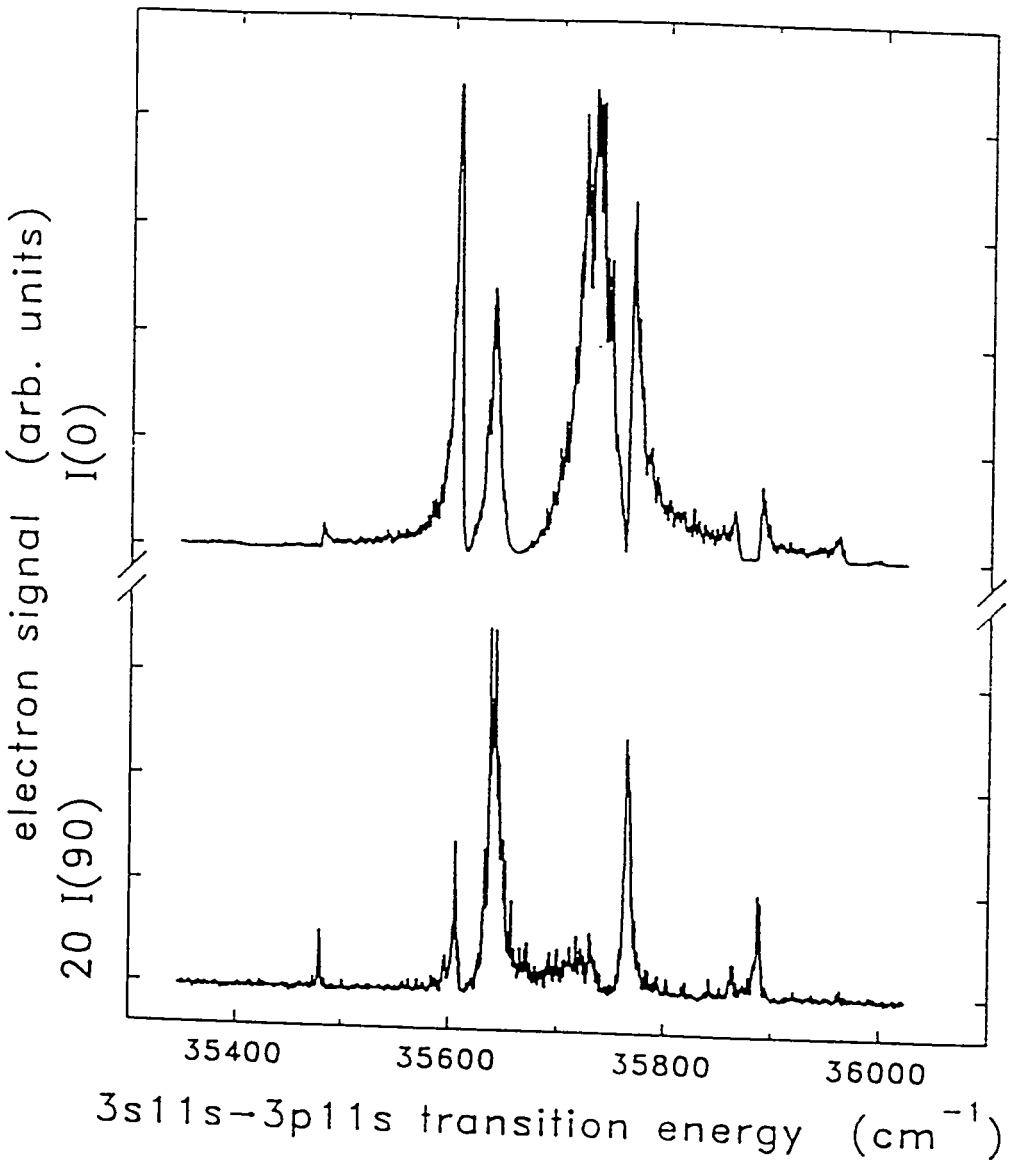

Fig. 1. Line shapes of the electron signal for the Mg 3s11s → 3p11s transition, detected simultaneously at two different angles θ. The top trace is I(θ=0°), and the bottom is I(θ=90°) multiplied by a factor of 20. I(θ=0°) and I(θ=90°) are used to derive the β parameter according to Eq. (2).

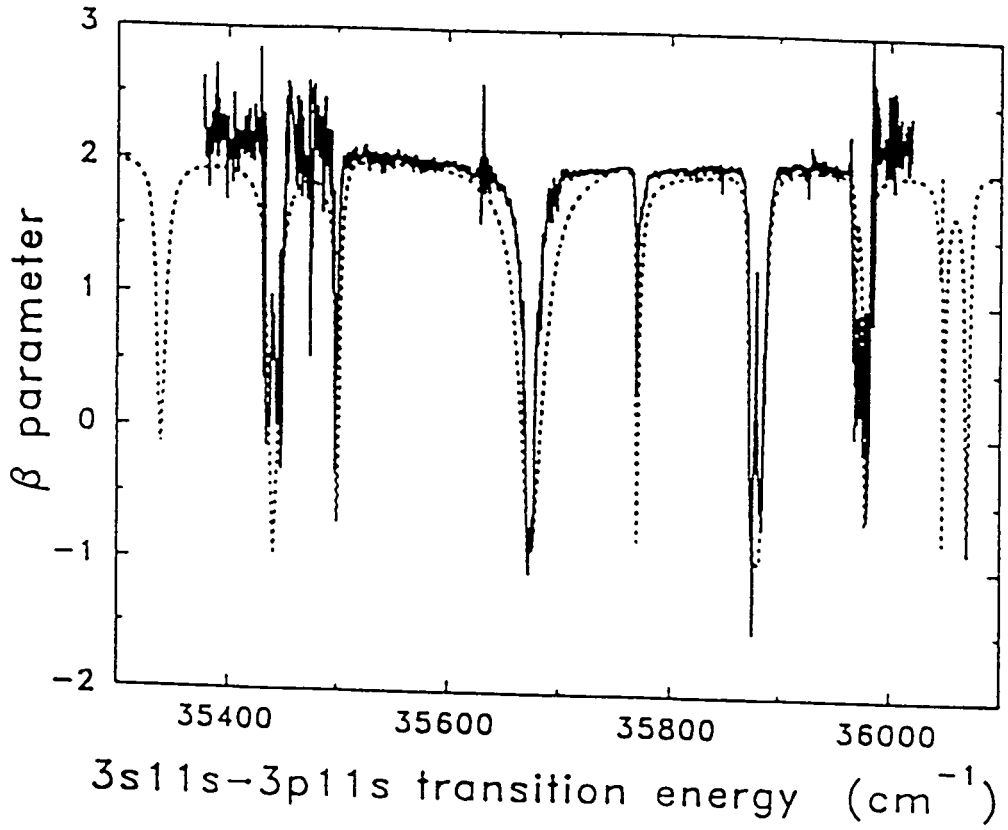

Fig. 2. The β parameter for the Mg 3s11s → 3p11s transition. The experimental results are shown with the solid line, and the predictions of the $\underline{K}$ matrix-MQDT theory are shown with the dotted line. In some parts of the graph the theoretical prediction is hidden under the data line.

that the experimental data are well reproduced by the K matrix calculations, shown by the dotted line.

The fact that β is typically near 2 shows that, in general, very little of the alignment put into the orbital motion is transferred to the two electrons' spins. At the other J=1 resonances angular momentum transfer between spin and orbital angular momenta occurs, producing the sharp decreases in β. On the other hand, it is less apparent why the β parameter exhibits the broad dip between the two Mg^+ resonance lines. A report of this work has been published in Physical Review A and is included as Appendix A.

Angular distributions of electrons from the Mg 3pnd states

There were two motivations for undertaking these measurements. First, this problem is intrinsically more challenging since we used the aligned Mg 3snd $^1D_2$ states as intermediate states. With three laser beams linearly polarized in the same direction the allowed final states are the 3pnd J=1 and J=3 states with m=0. Since the intermediate state is aligned, the angular distributions of the ejected electrons is given not by Eq. (2) but by

$$I(\theta) = \frac{I_0}{4\pi}\left[1 + \beta P_2(\cos\theta) + \gamma P_4(\cos\theta) + \epsilon P_6(\cos\theta)\right] , \qquad (3)$$

where θ is the angle between the laser polarizations and the momentum vector of the departing electron. The second motivation for these measurements is that they provide an even more stringent test of the K matrix calculations, for the results depend critically on both the J=1 and J=3 channels as well as the relative phases of the J=1 and J=3 wavefunctions.

The approach we used was essentially the same as the approach used to measure the angular distributions of electrons ejected from the Mg 3pns states. However, we used an ion detector and an electron detector, instead of two electron detectors. For a fixed value of θ we recorded the ion and electron signals as the wavelength of the third laser was scanned, and we computed the ratio of the electron to ion signals for each wavelength. We repeated this procedure for ten values of θ to build up the angular distributions of the ejected electrons.

Typical results obtained using the 3s12d state as the intermediate state, are shown in Fig. 3. There are several features of Fig. 3 worthy of note. First, β, γ, and ϵ, are generally positive, indicating that the electron is usually ejected in the direction of the lasers' polarization. Second, variations occur at resonances. Finally, the observed results are in excellent agreement with the K matrix calculations. To our knowledge these measurements is one of the most stringent tests of such calculations to date, and it is hard not to be impressed by the agreement between the calculated and observed spectra.

A useful way of looking at the parameters β, γ, and ϵ, is to decompose them into their J components. As an example we consider the β parameter. It can be decomposed into J=1, J=3, and mixed J components. As shown by Fig. 4, the J=1 and J=3 parts are positive almost everywhere, but the mixed J part is often negative. In other words, without the interference between the J=1 and J=3 channels the electrons would be ejected predominantly along the polarization axis of the lasers. It is the interference which often leads to ejection of the electron in the direction perpendicular to the laser polarization axis. A report of this work has been published in Physical Review A and is included as Appendix B.

Mg 3pnk autoionization rates in electric fields

Some of the cleanest measurements of dielectronic recombination are those made in Mg. In these measurements small electric fields were present, and they led to an increase in the recombination rate.[4,13] In addition, there have been calculations showing that fields increase the rate for dielectronic recombination.[14,15] We undertook these measurements to isolate the field effects. In Ba we observed that predictions of the Jacobs et al.[16,17] model were correct,[18] and, in addition, observed an n^{-4} scaling of autoionization rates in fields.[19,20] Since the Mg zero field spectra are so complex, it was not obvious that the spectra in electric fields would be as simple in Mg as they are in Ba.

The approach is straightforward. Mg atoms are excited to bound 3snk Stark states in a static field by two dye lasers. The wavelength of the third laser is then scanned in frequency. In Ba we observed

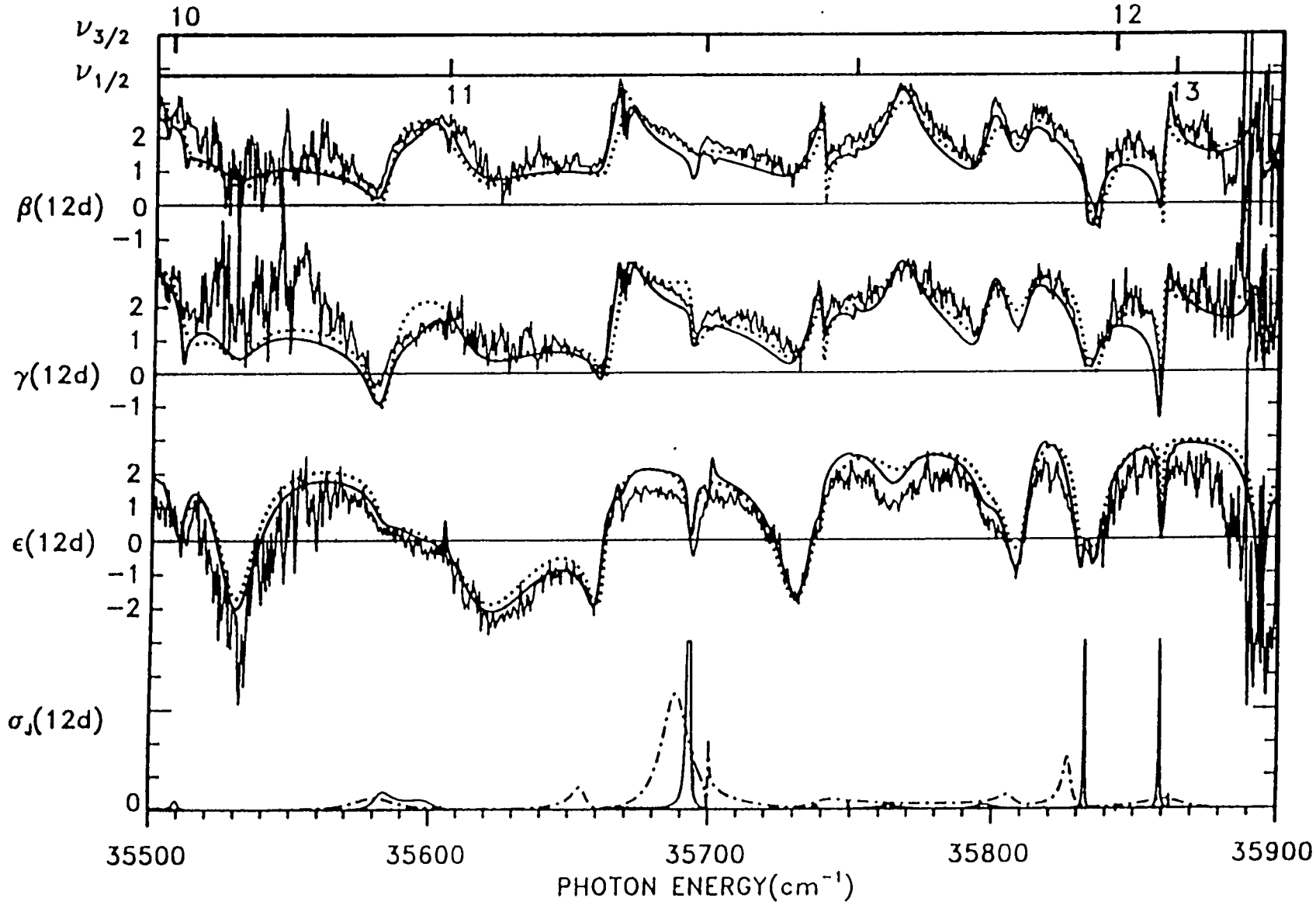

Fig. 3. Angular distribution parameters β, γ, and ϵ for the Mg 3s12d → 3p12d transitions.

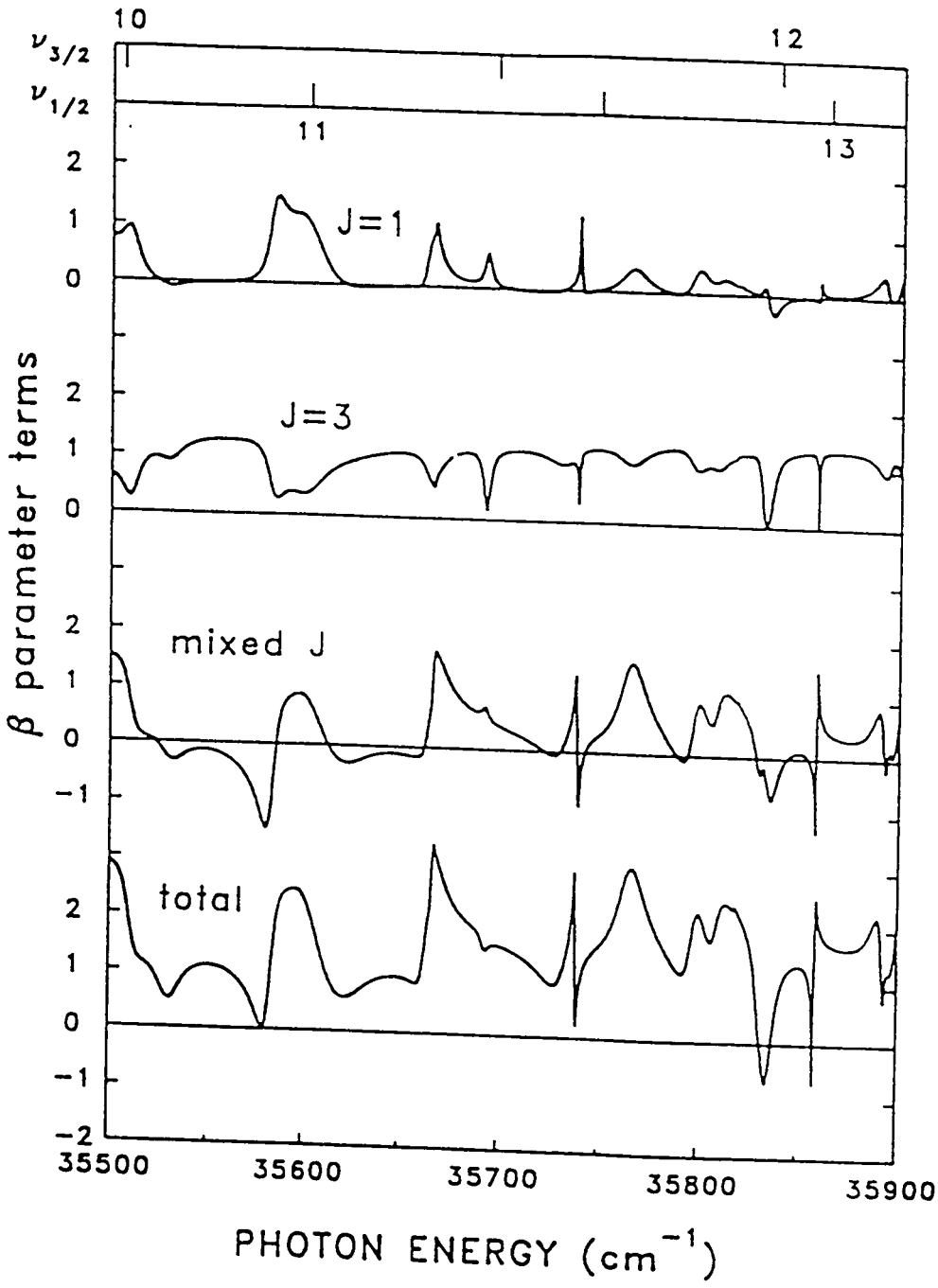

Fig. 4. Various contributions to the β parameter spectrum of the 3p12d state of Mg. In order from top to bottom, the graphs are of the contributions from only pure J=1 terms, from only pure J=3 terms, and from only mixed J terms. The bottom line is the complete β parameter, which is the sum of the top three graphs.

a single transition, from a bound 6snk Stark state to its autoionizing 6pnk analog. In Mg we usually see several transitions, not a single line. The spacings between the observed transitions do not match the spacing between the Stark states, and we have tentatively assigned the multiple peaks to Stark states converging to the other $3p_j$ limit. The widths of the autoionizing Stark states do not exhibit the $1/n^4$ scaling seen in Ba.[19,20] We attribute the clear difference between Ba and Mg to stronger interseries interactions in Mg than in Ba.

In the hope of clarifying the effects of fields we have examined the Mg Stark states in 12 GHz microwave fields. With a microwave field the 3snk - 3pnk excitation spectrum is reduced to two approximately Lorentzian peaks at the locations of the Mg^+ $3s_{1/2}$ - $3p_{1/2}$ and $3s_{1/2}$ - $3p_{3/2}$ transitions. This result is the same as obtained in Ba. What is not the same is that the linewidths of the transitions are independent of n, whereas in Ba we observed a clear n^{-4} scaling of the widths in a microwave field.

We find our results somewhat surprising, and quite interesting, in that they do not follow the easily understood pattern shown by Ba.

These measurements suggest that a description of the field effects based on an isolated resonance description may fail when there are overlapping series converging to different limits. We have prepared a report of this work, and it is included as Appendix C.

Autoionization of Ba 6pnk States in Electric Fields

During the period of this grant we have begun to record systematically the spectra of the Ba 6snk → 6pn'k' transitions with high optical power in static electric fields. The primary motivation for this work is to reach an understanding of the isolated core excitation spectra in fields which is comparable to our understanding of the zero field spectra. Specifically, we can describe the photoexcitation cross section in zero field as[21]

$$\sigma \propto |<6s|\mu|6p> <nd|\nu d> A(\nu)|^2 \qquad (4)$$

where ν is the effective quantum number of the 6pnd channel, $<6s|\mu|6p>$ is the constant Ba^+ dipole

matrix element, $<nd|\nu d>$ is the overlap integral for the outer electron, and $A(\nu)$ is the spectral density of the 6pnd channel of autoionizing states. The overlap integral has its large central lobe peaked where $\nu=n^*$, n^* being the effective quantum number of the 6snd states, and the spectral density has peaks at each autoionizing 6pnd state, with widths reflecting their autoionization rates. Due to the dominance of the central lobe of the overlap integral, the spectrum of Eq. (4) is dominated by a single resonance at $\nu \approx n^*$. However, it accounts quantitatively for changes in n of the outer electron as well.

When the 6snk → 6pnk transitions are observed with low optical power, so that the signal is proportional to the optical cross section, a single, approximately Lorentzian peak is observed. It is possible to explain the dominant peak of the observed resonance as arising from the 6snk → 6pnk resonance, i.e. ignoring the possibility of 6snk → 6pn'k' transitions in which $n' \neq n$ and $k' \neq k$. However, with higher power optical excitation the $n' \neq n$ and $k' \neq k$ transitions appear.

To describe spectra containing such transitions is much harder because the symmetry is lower than it is in zero field. It is no longer possible to restrict the final states to 6pnd channels as we have in Eq. (4). Fano has suggested an excellent way of approaching this problem, treating the outer electron near the ion core using spherical wavefunctions and far from the core using parabolic wavefunctions.[22] This approach has been applied very successfully to the spectra of alkali atoms in fields by Harmin,[23] and Sakimoto[24] has extended the method to excited states of the ionic core. Recently Armstrong et al.[25] have used this approach and have obtained excellent agreement between experimental and calculated Stark spectra of Ba in the autoionization region. In all of these calculations the initial state was one having small spatial extent, so the problem is somewhat easier than the isolated core excitation problem we face. Nonetheless, we are confident that the problem can be successfully treated.

Our initial goal has been to record the spectra of Ba 6snk → 6pn'k' transitions with high optical power to bring out the features due to $n' \neq n$ and $k' \neq k$ transitions. We have chosen Ba, not Mg, for two reasons. First, Ba has well separated Ba^+ $6p_{1/2}$ and $6p_{3/2}$ states so the problem reduces to a one limit

problem. Second, the Ba 6snk → 6pn'k' transitions are in the visible part of the spectrum, so it is straightforward to obtain enough optical intensity to observe weak 6snk → 6pn'k' features.

Our approach has been to excite Ba atoms in a beam. With two fixed frequency dye lasers we excite Ba from the ground $6s^2$ state to the 6s6p state and then to a 6snk Stark state. With a third laser we drive the 6snk → 6pn'k' transition. All three lasers are polarized parallel to an applied electric field, so only final states of m=0 are created. The excitation of the atoms occurs between field plates which also serve to expel the Ba^+ ions resulting from autoionization of the 6pnk states to the microchannel plate detector. The ion signal is recorded as the wavelength of the third laser is scanned.

As an example of our observations we consider the excitation of the nominal 6s17s state, which is adiabatically connected to the zerofield 6s17s state. This state is on the low energy side of the n=13 Stark manifold. At low power of the third laser we observe a single, approximately Lorentzian line at the ionic $6s_{1/2}$ - $6p_{3/2}$ frequency. It is the 6s17s → $6p_{3/2}$17s transition. At higher optical power, we see spectra such as the one shown in Fig. 5. The spectrum of Fig. 5 exhibits two interesting features. First, it has the overlap integral zeroes, as seen in the high power zero field spectra,[20] at detunings from the ion line of -260, -120, and +90 cm^{-1}, corresponding to changes in the outer electron's effective quantum number of -2, -1, and +1. The zeroes disappear at detunings of more than 100 cm^{-1} as the $6p_{3/2}$ns states lose their s character and merge with the Stark manifolds. Second, satellite features due to all the m=0 Stark states are quite evident. The n=12 Stark states are clearly visible at detunings from -100 to -60 cm^{-1}, the n=13 Stark states are plainly visible at detunings of 0 to 60 cm^{-1}, and the n=14 Stark states are visible at detunings from 100 to 150 cm^{-1}.

We are presently recording spectra such as the one shown in Fig. 5. As of the moment we can clearly state that while the Δk=0 transition may be the strongest, there is certainly no Δk=0 selection rule.

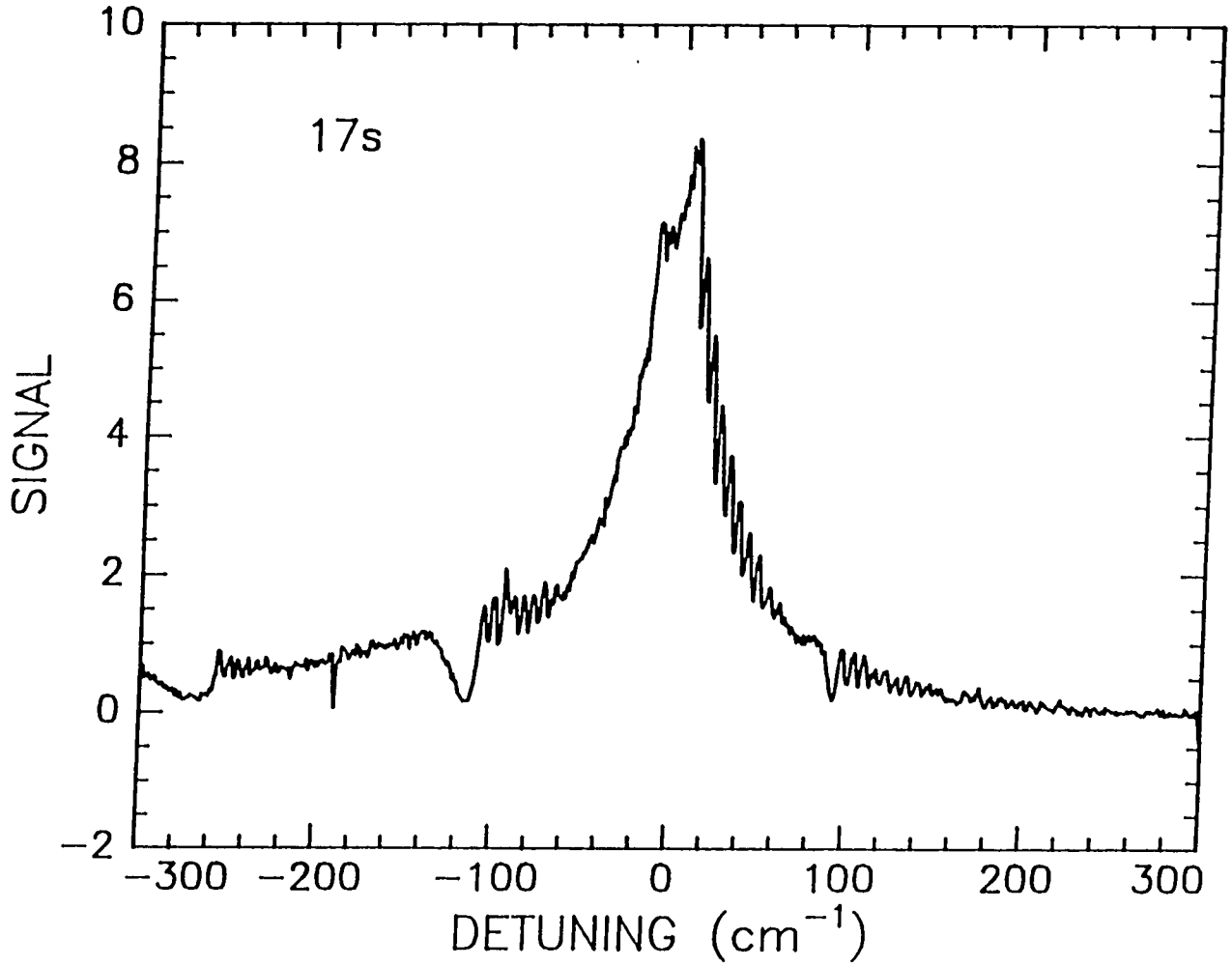

Fig. 5. Spectrum from the Ba 6s17s state to the $6p_{3/2}$ Stark states in a field of 3 kV/cm as a function of the detuning of the third laser from the $Ba^{+}6s_{1/2}$ - $6p_{3/2}$ ionic transition at 20261 cm^{-1}. Overlap integral zeroes are visible at detunings of -260, -110, and 90 cm^{-1}, but they are not visible at higher frequencies since the higher ns states have merged with the nearby Stark manifolds at this field. Satellites due to the n=12 Stark states are visible at detunings of -100 to -60 cm^{-1}. The n=13 and n=14 Stark state satellites occur at detunings in the ranges 0-60 cm^{-1} and 100-150 cm^{-1}.

Picosecond excitation of autoionizing states from bound wavepackets

A major undertaking in this grant period was the development of a picosecond laser system based on two synchronized ps dye lasers, and we are now beginning to reap the fruits of these labors. The first experiment we have carried out is the excitation of the Mg 3pnd autoionizing states from a wavepacket of bound 3snd states. This experiment shows explicitly the correlation between the wavelength of the light which is absorbed and the spatial location of the Rydberg electron when the light is absorbed, and to our knowledge it is the first experiment of its kind.

The experiment is based on two synchronized picosecond dye lasers. The two dye lasers are both pumped by the frequency doubled output of a continuous wave, mode locked Nd:YAG laser. Using this approach the timing jitter between the two dye laser pulses is inherently small, and we can routinely operate the lasers with less than 2 ps timing jitter. The fundamental of the Nd:YAG laser is used to seed a regenerative Nd:YAG laser which is used to pump three stage amplifiers for the two dye lasers. Typically we obtain 5 ps pulses from the dye lasers with 0.3 mJ pulse energies. For the Mg experiment the visible dye laser pulses are doubled to the ultraviolet in KDP crystals.

The basic notion of the experiment is shown in the energy level diagram of Fig. 6. Using two photon excitation we excite the bound Mg 3snd states of $n \sim 50$. Since the laser pulse is only 5 ps long, the laser pulse is over in a time much less than the round trip time, $2\pi n^3$, of the Rydberg electron. Consequently the laser pulse forms an outgoing wavepacket which is reflected from the coulomb potential at large r and returns to the core at integral multiples of the classical round trip time, which is 25 ps for $n = 50$. The above classical description can also be expressed in quantum mechanical terms. The initial laser pulse creates a coherent superposition of 3snd wavefunctions which interfere constructively at small orbital radius at $t = 0$. At integral multiples of the classical round trip time later the wavefunctions again add constructively at small orbital radius, and at half integral multiples of the classical roundtrip time later they add constructively at large orbital radius.

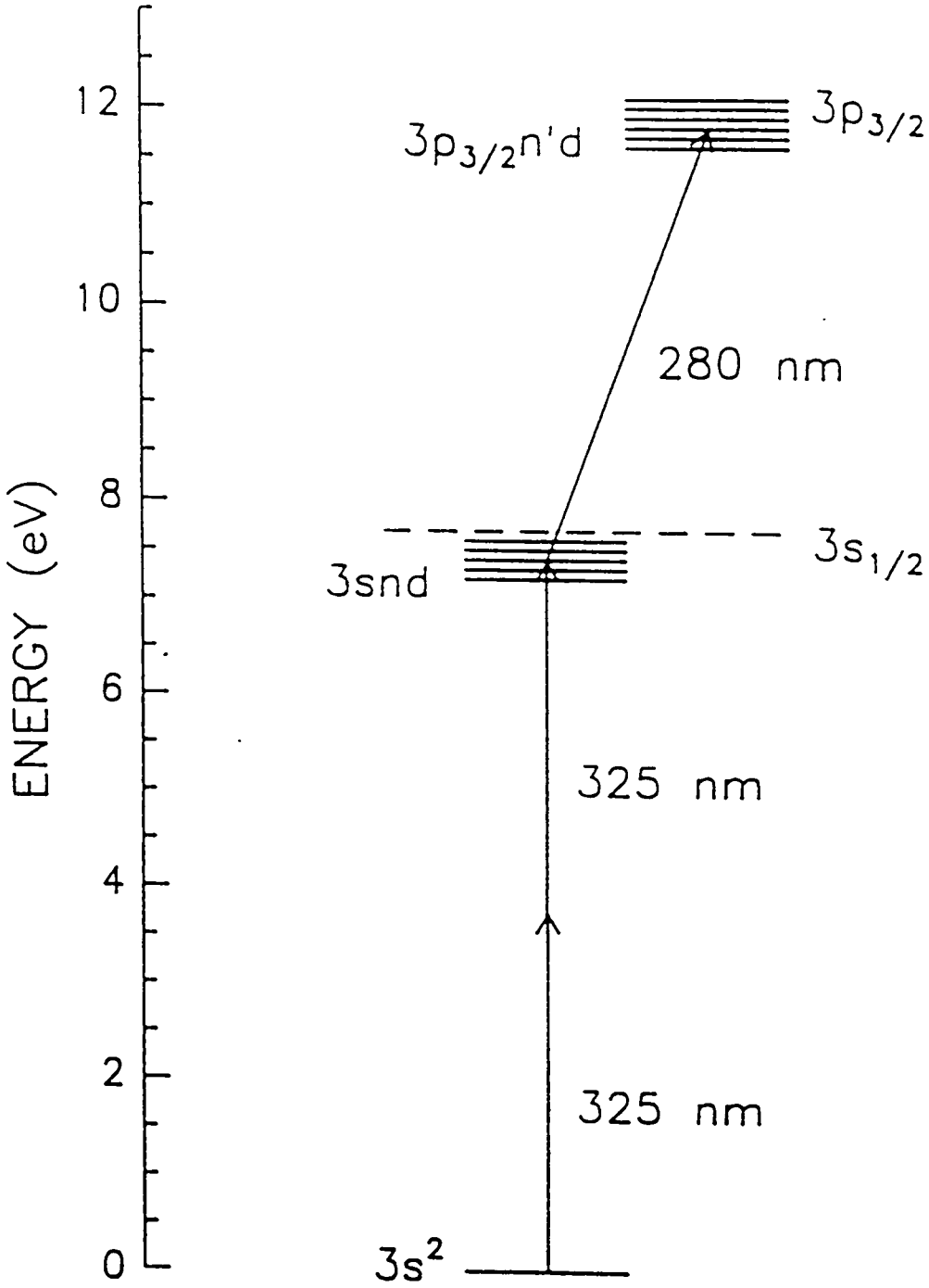

Fig. 6. The excitation path used in the experiment is shown. Two photons of doubled 650 nm light excited Mg to a 3snd $^1D_2$ Rydberg wave packet state, where n is the central state of the wave packet. One photon of the doubled 560 nm light then excited the 3s core electron, producing $3p_{3/2}n'd$ autoionizing states, where n′ is the central state of the final Rydberg wave packet.

The second picosecond laser, which drives the Mg^+ 3s-3p transition, is tuned on or off the $3s_{1/2}$ - $3p_{1/2}$ transition, and we monitor the production of Mg 3pnd atoms as the delay between the two lasers is scanned continuously. Specifically, we detect Mg^+ ions resulting from autoionization of 3pnd atoms. What we observe is shown in Fig. 7. As shown by Fig. 7(a), on resonance we observe a step function in the Mg^+ signal. If the second laser precedes the first we observe no Mg^+, since there are no bound Mg 3snd atoms to excite. If the second laser comes after the first the Mg^+ signal is independent of the delay, indicating that the excitation to the Mg 3pnd states can occur with the outer nd electron at any position in its orbit. In contrast, as shown by Figs. 7(b) and (c), if the laser is tuned off resonance we observe peaks in the Mg^+ signal when t = 0,26, and 52 ps, i.e. at integral multiples of the classical orbit time. When the second laser is off resonant the excitation can only occur when the Rydberg electron is near the ionic core because the outer electron must be near the ionic core to absorb or provide the energy by which the laser frequency is detuned from the Mg^+ transition frequency.

A report of this work has been published in Physical Review Letters and is included here as Appendix D.

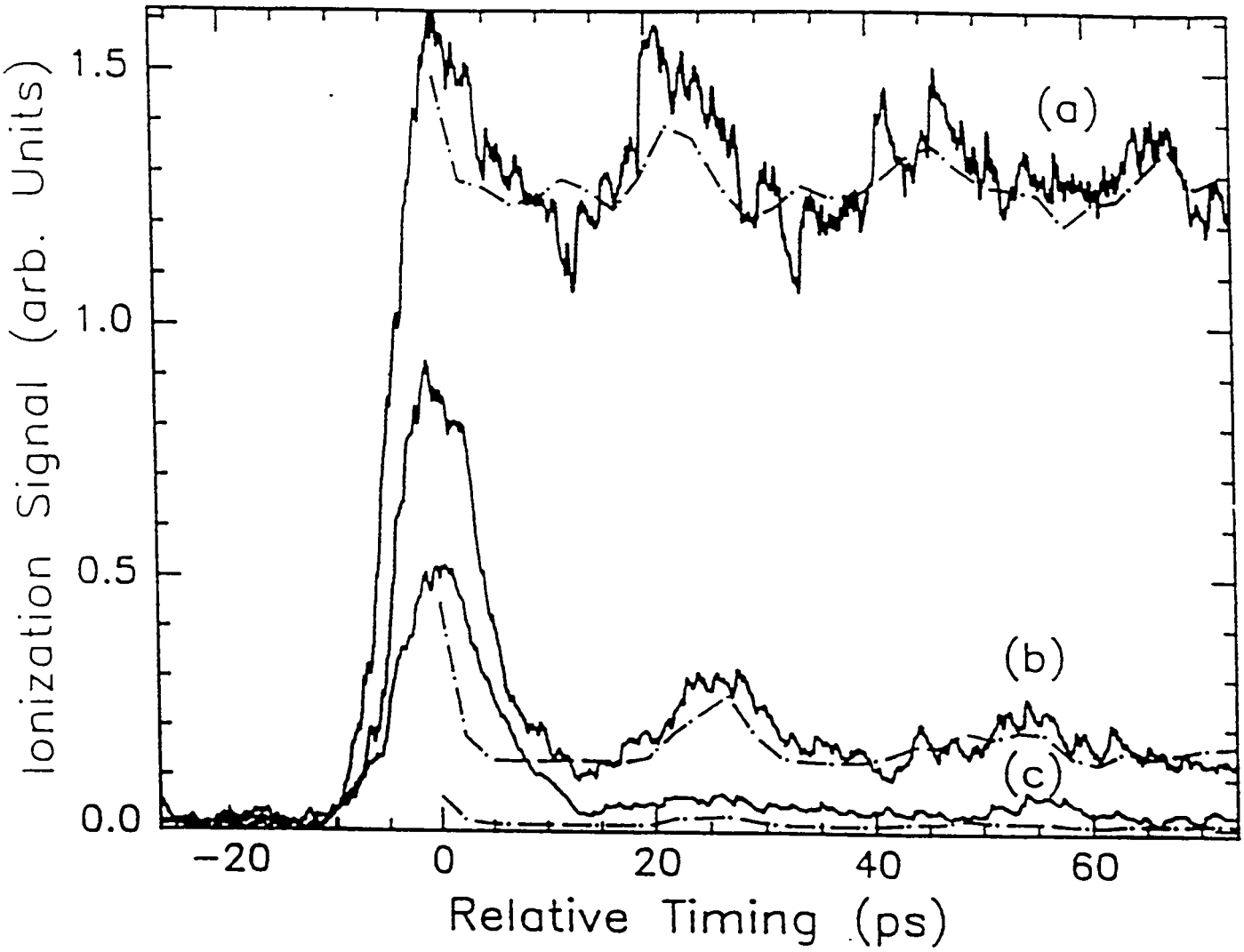

Fig. 7. Measured and calculated signals vs. delay time of the second pulse are shown for several tunings of the core laser with the Rydberg laser tuned to n=54. Near the ionic resonance, (a), the signal is essentially a step function, with the step at zero delay, indicating that the excitation of the core electron is independent of the position of the outer electron. When the second laser is detuned from the resonance, by 15 cm^{-1} in (b) and 30 cm^{-1} in (c), the excitation of the inner electron can only occur when the outer electron is at the ion core, hence the peaks in the signal at zero delay and multiples of the classical round trip time, 26 ps.

IV. References

1. Y. Hahn, in Advances in Atomic and Molecular Physics Vol. 21, eds. D. Bates and B. Bederson (Academic, New York, 1985).

2. J.S. Dubau and S. Volonté, Rep. Prog. Phys. 43, 199 (1980).

3. S.E. Harris, Opt. Lett. 5, 1 (1980).

4. D.S. Belic, G.H. Dunn, T.J. Morgan, D.W. Mueller, and C. Timmer, Phys. Rev. Lett. 50, 339 (1983).

5. L. Kim and C.H. Greene, Phys. Rev. A 36, 4272 (1987).

6. C.H. Greene (private communication).

7. W.E. Cooke, T.F. Gallagher, S.A. Edelstein and R.M. Hill, Phys. Rev. Lett. 40, 178 (1978).

8. A. Lindgard and S.E. Nielsen, Atomic Data and Nuclear Data Tables 19, 534 (1977).

9. U. Fano, Phys. Rev. 124, 1866 (1961).

10. C.J. Dai, G.W. Schinn, and T.F. Gallagher, Phys. Rev. A 42, 223 (1990).

11. G.W. Schinn, C.J. Dai, and T.F. Gallagher, Phys. Rev. A 43, 2316 (1991).

12. C.N. Yang, Phys. Rev. 74, 764 (1948).

13. G.H. Dunn, D.S. Belic, B. DePaola, N. Djuric, D. Mueller, A. Muller, and C. Timmer, in Atomic Excitation and Recombination in External Fields, eds. M.H. Nayfeh and C.W. Clark (Gordon and Breach, New York, 1985).

14. K. LaGattata and Y. Hahn, Phys. Rev. Lett. 51, 558 (1983).

15. D.C. Griffin, M.S. Pindzola, and C. Bottcher, Phys. Rev. A 33, 3124 (1986).

16. V.L. Jacobs, J. Davis and P.C. Kepple, Phys. Rev. Lett. 37, 1390 (1976).

17. V.L. Jacobs and J. Davis, Phys. Rev. A 18, 697 (1978).

18. K.A. Safinya, J.F. Delpech, and T.F. Gallagher, Phys. Rev. A 22, 1062 (1980).

19. S.M. Jaffe, R. Kachru, H.B. van Linden van den Heuvell, and T.F. Gallagher, Phys. Rev. A 32, 1480 (1985).

20. R.R. Jones and T.F. Gallagher, Phys. Rev. A 39, 4583 (1989).

21. N.H. Tran, P. Pillet, R. Kachru, and T.F. Gallagher, Phys. Rev. A 29, 2640 (1984).

22. U. Fano, Phys. Rev. A 24, 619 (1981).

23. D. Harmin, Phys. Rev. Lett. 49, 128 (1982).

24. K. Sakimoto, J. Phys. B 19, 3011 (1986).

25. D.J. Armstrong, C.H. Greene, R.P. Wood, and J. Cooper, Phys. Rev. Lett. 70, 2379 (1993).